Thermal and physico-chemical studies on binary organic eutectic systems

4-Aminoacetophenone with benzoin and 4-nitrophenol

Shiva Kant · U. S. Rai · R. N. Rai

Abstract The phase diagrams of binary systems of 4-aminoacetophenone (AAP) with each of benzoin (BN) and 4-nitrophenol (PNP) have been established by the thaw-melt method. This study shows the formation of eutectics. Accurate compositions of BN and PNP to form eutectic mixtures have been determined by the phase diagram study between BN–AAP and PNP–AAP in the entire range of compositions. The thermal properties of the eutectics, such as enthalpy of mixing, solid–liquid interfacial energy, entropy of fusion and excess thermodynamic functions were computed based on enthalpy of fusion values. The influence of undercooling on growth kinetics of pure components and their eutectics has been studied. The microstructural studies infer the influence of solid–liquid interfacial energy on the morphology of microstructures of eutectics.

Keywords Phase diagram · Eutectics · Growth kinetics · Heat of mixing · Excess thermodynamic functions

Introduction

The eutectic alloys are found competent materials for the supersonic aircraft, space vehicles, high pressure tanks, thermoelectric devices (safety plugs in fire detection apparatus, alarm signals, etc.), and production of permanent magnets. Superalloy eutectics are found to be the promising construction materials for sophisticated turbines and vanes. One of the most attractive methods of producing high-strength composite materials is by unidirectional solidification [1–3]. This type of solidification process can produce materials with interesting mechanical, electronic, optical, and magnetic properties. Metallic systems [4, 5] constitute an interesting area of investigations but they are not suitable for detailed study due to wide density difference, opacity and high transformation temperature of the components involved. However, low transformation temperature, transparency, wider choice of materials and minimized convection effects are the special features that have prompted a number of research groups to work on organic eutectics, monotectics and molecular complexes [6, 7]. As such, organic systems are used as model systems for detailed investigation of several parameters which control the mechanism of solidification and subsequently decide the properties of materials. However, the last two decades have witnessed the use of organic compounds for binary synthesis and their physicochemical investigations as they are potential materials for nonlinear optical (NLO), electro-optic, conductors and different other electronic applications [8–10]. The technique of molecular complexation has been developed as one of the designing tools in molecular crystal engineering of noncentrosymmetric structures [11, 12]. Furthermore, the technique of binary preparation of organic materials has been found capable of modifying the drawbacks of several organic materials to make them worth for device application [13, 14].

In the present paper, the data on two systems, namely, BN–AAP and PNP–AAP related to their phase diagram, thermochemical properties, growth kinetics and microstructural studies of the parent components and eutectics are reported.

S. Kant · U. S. Rai · R. N. Rai (✉)
Department of Chemistry, Centre of Advanced Study,
Banaras Hindu University, Varanasi 221 005, India
e-mail: rn_rai@yahoo.co.in

Experimental

Purification of materials

The starting material 4-aminoacetophenone (Sigma-Aldrich, Germany) was purified by recrystallization in chloroform [15], while benzoin (Sigma-Aldrich, Germany) was purified by recrystallization from carbon tetrachloride and 4-nitrophenol (Sd. Fine, India) was purified by repeated distillation under reduced pressure and stored in amber-colored bottles to avoid exposure to light [16]. The purity of each compound was assessed by measuring their melting points.

Phase diagram

The phase diagram of BN–AAP and PNP–AAP systems were determined by the thaw-melt method and established in the form of a temperature-composition curve [17]. Mixtures of the parent components covering entire range of compositions were prepared and their melts were homogenized by continuous shaking, followed by chilling in ice cold water. The melting temperature of each composition was recorded using Toshniwal melting point apparatus attached with a precision thermometer (± 0.5 °C).

Enthalpy of fusion

The enthalpy of fusion of the pure components and the eutectics were determined by a differential scanning calorimeter (Mettler DSC-4000 system). The indium and zinc samples were used to calibrate the DSC unit. The amount of sample and the heating rate were about 5–7 mg and 10 °C min^{-1}, respectively.

Growth kinetics

The influence of temperature on growth kinetics of the pure components and their eutectics were studied [18, 19] by measuring the rate of movement of the solid–liquid interface at different undercoolings in a U-shape tube of 150 mm horizontal portion and 5 mm internal diameter. Molten samples of the pure components and the eutectics were separately taken in a capillary and placed in a silicone oil bath. The temperature of the oil bath was maintained using microprocessor temperature controller of accuracy ± 0.1 °C. At a particular undercooling, below the melting point of the sample, a seed crystal of the same composition was added to start the nucleation process and the rate of movement of the solid–liquid interface was measured using a traveling microscope and a stop watch.

Microstructure

Microstructures of the pure components and their eutectics were recorded [20] by placing a drop of molten compound on a hot glass slide. To avoid the inclusion of the impurities from the atmosphere, a cover slip was glided over the melt and it was allowed to cool to get a super-cooled liquid. The melt was nucleated with a seed crystal of the same composition at one end, taking care to have unidirectional freezing. The directionally solidified structure was then placed on the platform of an optical microscope (Leitz Labourlux D). The different regions of the slide were viewed and photographs of interesting region were taken using suitable magnification of camera attached with the microscope.

Results and discussion

Phase diagram

The phase diagram of BN–AAP and PNP–AAP systems, reported in terms of temperature-composition curves show the formation of simple eutectics which have been shown in Figs. 1 and 2, respectively. The melting temperatures of BN and PNP are 135 and 114 °C, respectively. The melting temperatures of both BN and PNP decrease with the addition of AAP. The minimum melting temperature for BN–AAP having 0.8 mol composition of AAP is 93 °C. Similarly in case of PNP–AAP, the melting temperature of PNP (114 °C) decreases with the addition AAP, and reaches to the minimum (80 °C). At the eutectic temperature (T_{E}), the two solid phases S_1 and S_2 and a liquid solution of the two components (L) are in equilibrium, and therefore the point E of each system is an invariant point. At the eutectic point, just below the eutectic temperature, both components separate out from the liquid phase of eutectic composition to two solid phases.

$$L \rightleftharpoons S_1 + S_2 \tag{1}$$

The L + S region of both the systems are monovariant. In the area indicated by L, a homogeneous binary liquid solution exists while the two solid phases S_1 and S_2 exist below the eutectic horizontal line.

The homogeneous regions of both systems are bivariant. In each case, in the L + S_1 region which is above the eutectic point and located on the left side of the diagram, a binary liquid L and a solid S_1 coexist. Similarly, in the L + S_2 region located on the right side of each diagram, a binary liquid L and a solid S_2 coexist. The binary liquid denoted by L, on the left hand side liquid is rich in the component indicated on the left hand ordinate while liquid
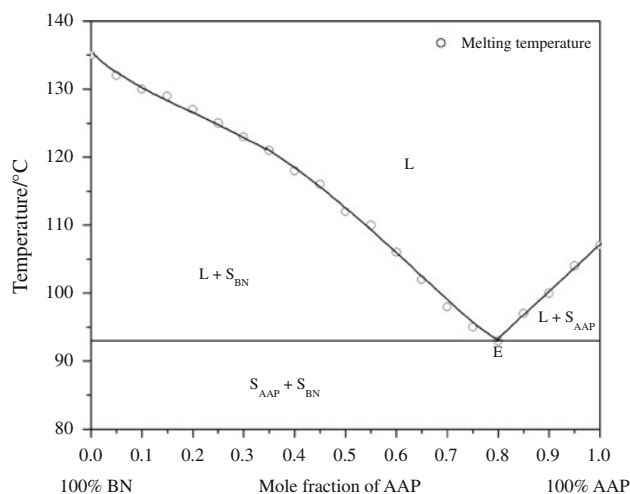
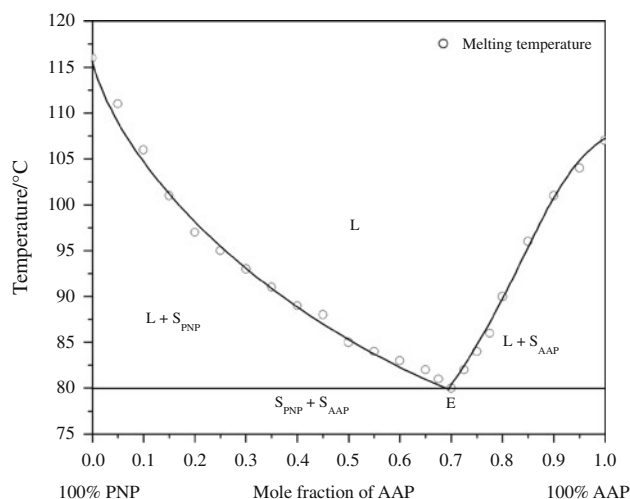Fig. 1 Phase diagram of benzoin and 4-aminoacetophenone

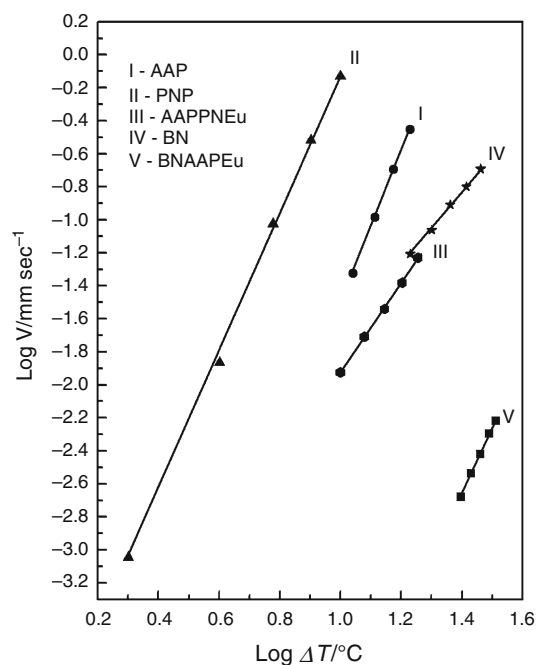Fig. 2 Phase diagram of 4-nitrophenol and 4-aminoacetophenone

Fig. 3 Linear velocity of crystallization of BN, AAP, PNP, and their eutectics

Table 1 Values of u and n for pure components BN, AAP, PNP, and their eutectics

Materials	n	u/mm sec^{-1} deg^{-1}
BN	2.23	1.09×10^{-4}
AAP	4.61	7.53×10^{-7}
PNP	4.35	3.77×10^{-5}
BN–AAP Eu	4.00	5.37×10^{-9}
PNP–AAP Eu	2.70	2.37×10^{-5}

phase (L) of the right hand side is rich in the other component shown on the right hand ordinate.

Growth kinetics

In order to study the crystallization behavior of the pure components and their eutectics, the crystallization rate (v) is determined at different undercoolings (ΔT) by measuring the rate of movement of solid–liquid interface in a capillary. The plots between log ΔT and log v are given in (Fig. 3). The linear dependence of these plots is in accordance with the Hillig and Turnbull [21] equation,

$$v = u(\Delta T)^n \qquad (2)$$

where u and n are constants and depend on the solidification behavior of the materials involved. The values of u and n are given in Table 1. The findings may be explained by the mechanism given by Winegard et al. [22].

According to them, the crystallization of eutectic begins with the formation of the nucleus of one of the phases. This phase grows until the surrounding liquid becomes rich in the other component and a stage is reached when the second component also starts nucleating. Thus, there are two possibilities, either the two initial crystals grow side-by-side or they may grow by alternate nucleation of the two phases. The values of n being close to 2 suggest the square relationship between growth and undercooling (ΔT). The deviation of n values from 2, observed in some cases, is due to difference in temperature of bath and temperature of growing interface. From the values of u (Table 1) it can be concluded that growth velocity of eutectics is lower than the parent components. These findings suggest that the two phases of eutectics solidify by the side-by-side growth mechanism.

Thermochemistry

The knowledge of enthalpy of fusion values of the pure components and their eutectics is important in understanding the mechanism of solidification, structure of eutectic melt, and the nature of interaction between two components forming the eutectics. The values of enthalpy of fusion of the pure components and their eutectics, determined by the DSC method, are reported in Table 2. For comparison, the values of enthalpy of fusion of eutectics calculated by the mixture law [17] are also included in the same table. The values of enthalpy of mixing which is the difference between experimental and the calculated values of the enthalpy of fusion of the eutectics are found to be −7.05 and −1.35 kJ/mol for BN–AAP and PNP–AAP systems, respectively. Three possible structures are suggested [23]; quasi-eutectic for $\Delta_{mix}H > 0$, clustering of molecules for $\Delta_{mix}H < 0$, and molecular solution for $\Delta_{mix}H = 0$. In the present systems, the negative value of $\Delta_{mix}H$ for the eutectics suggests that there is an associative interaction in the molecules in eutectic melt [24]. The entropy of fusion ($\Delta_{fus}S$) values, for different materials, has been calculated by dividing the enthalpy of fusion by their corresponding absolute melting temperatures (Table 2). The positive values suggest that the entropy factor favors the melting process.

The deviation from the ideal behavior can best be expressed in terms of excess thermodynamic functions, namely, excess free energy (g^E), excess enthalpy (h^E), and excess entropy (s^E) which give more quantitative idea about the nature of molecular interactions. The excess thermodynamic functions could be calculated [17, 24] using the following equations and the values are given in Table 3:

Table 2 Heat of fusion, entropy of fusion, and roughness parameters of the systems

Materials	Enthalpy of fusion/ kJ mol^{-1}	Heat of mixing/ kJ mol^{-1}	Entropy of fusion/ J mol^{-1}/K	Roughness parameters/ α
BN	40.30		98.80	11.88
AAP	17.86		46.87	5.64
PNP	19.22		49.00	5.89
Eutectic (Exp.)	15.30	−7.05	41.80	5.03
(BN–AAP) (Cal.)	22.35			
Eutectic (Exp.)	16.92	−1.35	48.00	5.77
(PNP–AAP) (Cal.)	18.27			

Table 3 Excess thermodynamic functions for the eutectics of BN–AAP and PNP–AAP

Material	g^E/kJ mol^{-1}	h^E/kJ mol^{-1}	s^E/kJ mol^{-1}/K
BN–AAP eutectic	0.133	19.490	0.053
PNP–AAP eutectic	0.398	20.513	0.057

$$g^E = RT\left[x_1 \ln\gamma_1^l + x_2 \ln\gamma_2^l\right] \tag{3}$$

$$h^E = -RT^2\left[x_1 \frac{\partial \ln\gamma_1^l}{\partial T} + x_2 \frac{\partial \ln\gamma_2^l}{\partial T}\right] \tag{4}$$

$$s^E = -R\left[x_1 \ln\gamma_1^l + x_2 \ln\gamma_2^l + x_1 T \frac{\partial \ln\gamma_1^l}{\partial T} + x_2 T \frac{\partial \ln\gamma_2^l}{\partial T}\right] \tag{5}$$

where $\ln\gamma_i^l$, x_i, and $\frac{\partial \ln\gamma_i^l}{\partial T}$ are activity coefficient in the liquid state, the mole fraction, and the variation of log of activity coefficient in liquid state as a function of temperature of the component i, respectively.

It is evident from equations, (3)–(5), that activity coefficient and its variation with temperature is required to calculate the excess functions. Activity coefficient (γ_i^l) could be evaluated [17, 20] using the equation,

$$-\ln\left(x_i \gamma_i^l\right) = \frac{\Delta_{fus}H_i}{R}\left(\frac{1}{T_{fus}} - \frac{1}{T_i}\right) \tag{6}$$

where x_i, $\Delta_{fus}H_i$, T_i, and T_{fus} are mole fraction, enthalpy of fusion, melting temperature of component i, and melting temperature of eutectic, respectively. The variation of activity coefficient with temperature could be calculated by differentiating equation (6) with respect to temperature

$$\frac{\partial \ln\gamma_i^l}{\partial T} = \frac{\Delta_{fus}H_i}{RT^2} - \frac{\partial x_i}{x_i \partial T} \tag{7}$$

$\partial x_i/\partial T$ in this expression can be evaluated by considering two points around the eutectic. The positive values of excess free energy for both cases of eutectics indicate that the interaction between the like molecules (BN–BN, AAP–AAP, and PNP–PNP) are stronger than the interaction between the unlike molecules (BN–AAP and PNP–AAP).

The solid–liquid interfacial tension affects the enthalpy of fusion value and plays an important role in determining the kinetics of phase transformation [25]. When liquid is cooled below its melting temperature, the melt does not solidify spontaneously because under equilibrium condition, it contains number of clusters of molecules of different sizes. As long as the clusters are well below the critical size [26], they cannot grow to form crystals and, therefore, no solid would result. Also during growth, the radius of critical nucleus gets influenced by undercooling

Table 4 Interfacial energy and grain boundary energy of BN, AAP, PNP, and their eutectics

Parameter	Interfacial energy $\times 10^{-3}$/J m^{-2}	Grain boundary energy $\times 10^{-3}$/J m^{-2}
σ_{SL_1} (BN)	64.23	128.46
σ_{SL2} (AAP)	36.27	72.54
σ_{SL_1} (PNP)	44.00	88.00
σ_{E} (BN–AAP)	45.40	90.80
σ_{E} (PNP–AAP)	37.67	75.38

and interfacial energy as well. The interfacial energy (σ) is given by

$$\sigma = \frac{C \cdot \Delta_{fus}H}{(N_A)^{1/3} (V_m)^{2/3}} \tag{8}$$

where N_A is the Avogadro number, V_m is the molar volume, and parameter C lies between 0.35 and 0.45. The calculated values of interfacial energy for both systems are given in Table 4.

The grain boundary energy of the binary materials is also computed with the help of interfacial energy. In a polycrystalline material, a grain boundary is the interface between two grains which are oriented in different fashion. Grain boundaries disrupt the motion of dislocations through a material and play an important role [27, 28]. On the other hand, the grain boundaries tend to decrease the electrical and thermal conductivity of the material. The high interfacial energy and relatively weak bonding along the grain boundaries very often makes a preferred site for the onset of corrosion and for the precipitation of new phases from the solid. The grain boundary energy (γ) is related with interfacial energy and grain boundary angle by the relation [29],

$$\gamma = 2\sigma \cos\theta \tag{9}$$

where θ is the angle between tangents on interface and is known as grain boundary angle. The determination of the exact value of θ is complicated, however, the range of grain boundary energy could be approximated because the value of $\cos\theta$ may be less than or equal to one, and thus the value of grain boundary energy will be less than or equal to twice the interfacial energy.

To determine the size of the critical nucleus (r^*) and the influence of undercooling on it, the following equation was used:

$$r* = \frac{2\,\sigma\,T_{fus}}{\Delta_{fus}H \cdot \Delta T} \tag{10}$$

where T_{fus}, $\Delta_{fus}H$, and ΔT are melting temperature of eutectic, heat of fusion, and degree of undercooling,

Table 5 Critical radius of the BN, AAP, PNP, and their eutectics

Undercooling ΔT/°C	Critical radius $\times 10^{-9}$/cm				
	BN	AAP	PNP	Eutectic (BN–AAP)	Eutectic (PNP–AAP)
2.0			88.59		
4.0			44.29		
6.0			29.53		
8.0			22.15		
10.0			17.72		
11.0					15.73
11.5		14.10			
12.0					13.10
13.0		11.90			
14.0					11.23
15.0		10.30			
16.0					9.83
17.0	7.65	9.10			
18.0					8.74
20.0	6.50				
23.0	5.65				
25.0				8.70	
27.0				8.04	
29.0	4.48			7.49	
31.0				7.00	
33.0				6.58	

respectively. The computed values of the size of critical nucleus at different undercoolings using the equations (8) and (10) for both systems are given in Table 5. The size of critical nucleus decreases with increase in undercooling. Thus, high undercooling favors the formation of critical nucleus of smaller size. This may be ascribed to the increase in amplitude of molecular vibration at higher temperature.

Microstructure

It is well known that in polyphase materials the microstructure gives information about shape and size of the crystallites, which play a very significant role in deciding mechanical, electrical, magnetic, and optical properties of materials. According to Hunt and Jackson [30], the type of growth from melts depends upon the interface roughness (α) defined by

$$\alpha = \xi\Delta_{fus}H/RT \tag{11}$$

where ξ is a crystallographic factor which is generally equal to or less than one. The calculated values of α are reported in Table 2. If $\alpha > 2$ the interface is quite smooth and the crystal develops with a faceted morphology. On the
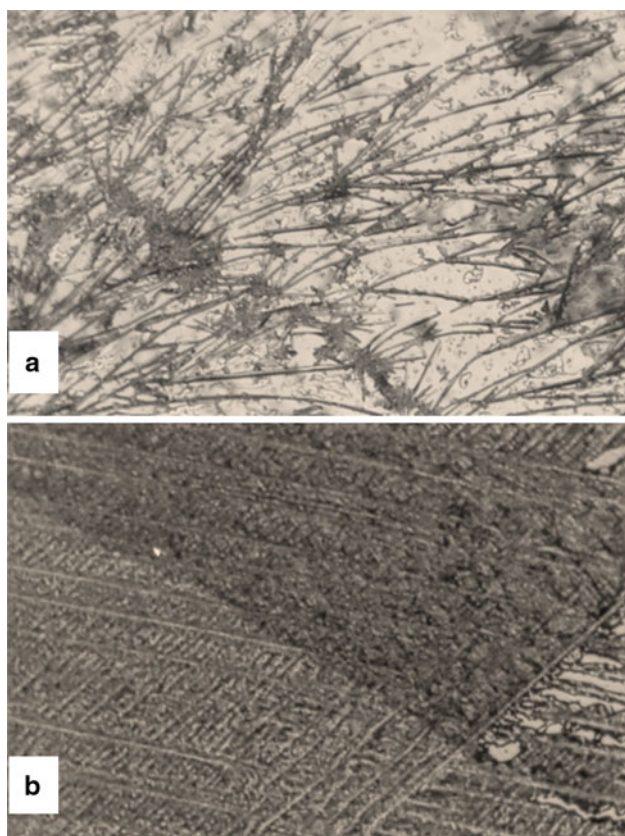
Fig. 4 Microstructure of directionally solidified **a** BN–AAP eutectic and **b** PNP–AAP eutectic

other hand, if $\alpha < 2$, the interface is rough and many sites are continuously available and the crystal develops with a non-faceted morphology. In the present systems, the values of α are >2 in all the cases suggesting thereby that the phases grow with facets morphology. The value of α for all the parent components BN, AAP, PNP, and their eutectics are higher than 2 suggesting their faceted growth. The microphotograph of BN–AAP eutectic (Fig. 4a) shows the dendritic growth which has maintained unidirectional growth. The eutectic microstructure of PNP–AAP (Fig. 4b) shows the fibrous growth which could be divided in different parts.

Conclusions

The phase diagram of BN–AAP and PNP–AAP systems shows the formation of simple eutectics with 0.8 and 0.7 mol fraction of AAP, respectively. The composition of eutectic mixtures has been determined by establishing their respective phase diagrams in the entire range of compositions. The melting temperature of eutectics of BN–AAP and PNP–AAP are 93.0 and 80.0 °C, respectively. The computed thermal properties and excess thermodynamic

functions of pure components and their eutectics based on enthalpy of fusion values, show associative interaction between molecules forming eutectics. The microstructure of eutectics shows the dendrite and fibrous morphology.

References

1. Mota MA, Coelho AA, Bejaraho JMZ, Gama S, Caram R. Directional growth and characterization of Fe–Al–Nb eutectic alloys. J Cryst Growth. 1999;198(199):850–5.
2. Pan Y, Sun GX. Directional solidification and magnetic properties of MnSb–Sb eutectic composite. J Mater Sci. 1998;33:763–8.
3. Caram R, Milenkovic S. Microstructure of Ni–Ni$_3$Si eutectic alloy produced by directional solidification. J Cryst Growth. 1999;198(199):844–9.
4. Trivedi R, Kurz W. Dendritic growth. Int Mater Rev. 1994;39(2): 49–74.
5. Glicksman ME, Singh NB, Chopra M. Gravitational effect in dendritic growth. Manuf Sp. 1983;11:207–18.
6. Reddi RSB, Satuluri VSA Kumar, Rai US, Rai RN. Thermal, physicochemical and microstructural studies of binary organic eutectic systems. J Therm Anal Calorim. 2012; 107: 377–85.
7. Gupta RK, Singh RA. Thermochemical and microstructural studies on binary organic eutectics and complexes. J Cryst Growth. 2004;267:340–7.
8. Farges JP. Organic conductors. New York: Marcel Dekker Inc.; 1994.
9. Gunter P. Nonlinear optical effects and materials. Berlin: Springer; 2000. p. 540.
10. Singh NB, Henningsen T, Hopkins RH, Mazelsky R, Hamacher RD, Supertzi EP, Hopkins FK, Zelmon DE, Singh OP. Nonlinear optical characteristics of binary organic system. J Cryst Growth. 1993;128:976–80.
11. Muthuraman M, Masse R, Nicoud JF, Desiraju GR. Molecular complexation as a design tool in the crystal engineering of non-centrosymmetric structures. Ideal orientation of chromophores linked by O–H⋯O and C–H⋯O hydrogen bonds for nonlinear optics. Chem Mater. 2001;13:1473–9.
12. Rai RN, Lan CW. Crystal structure and properties of new organic nonlinear optical material. J Mater Res. 2002;17(7):1587–91.
13. Lal RB, Chang JM, Batra AK. Growth and properties of urea doped triglycine sulphate (UrTGS). J Cryst Growth. 1996;158: 284–8.
14. Rai RN, Ramasamy P, Lan CW. Synthesis and crystal growth of binary organic NLO material UNBA. J Cryst Growth. 2002;235: 499–504.
15. Armarego WLF, Parrin DD. Purification of laboratory chemicals. 4th ed. Oxford: Butterworth-Heinemann Elsevier; 1999. p. 84.
16. Oliver K, Segur JB, Clarke HT, Taylor ER. Organic Syntheses. Coll. Vol. 1, p. 391 (1941); Vol. 3, p. 73 (1923).
17. Rai RN. Phase diagram, optical, nonlinear optical, and physico-chemical studies of the organic monotectic system: penta-chloropyridine-succinonotrile. J Mater Res. 2004;19(5):1348–55.
18. Rai US, Rai RN. Physical chemistry of organic eutectic and monotectic: hexamethylbenzene-succinonitrile system. Chem Mater. 1999;11(11):3031–6.
19. Rai US, Rai RN. Physical chemistry of organic eutectics. J Therm Anal Calorim. 1998;53:883–93.
20. Reddi RSB, Kant Shiva, Rai US, Rai RN. Crystallization, thermal, phase diagram and microstructural studies of organic analog

of metal–non metal monotectic alloy: 4-bromochlorobenzene–succinonitrile. J Cryst Growth. 2009;312:95–9.

21. Hillig WB, Turnbull D. Theory of Crystal growth in undercooled pure liquids. J Chem Phys. 1956;24:914.

22. Winegard WC, Majka S, Thall BM, Chalmers B. Eutectic solidification in metals. Can J Chem. 1951;29:320–7.

23. Rai RN, Rai US. Solid–liquid equilibrium and thermochemical properties of organic eutectic in a monotectic system. Thermochim Acta. 2000;363:23–8.

24. Singh N, Singh Narsingh B, Rai US, Singh OP. Structure of eutectic melts; binding organic systems. Thermochim Acta. 1985;95:291–3.

25. Eustathopoulos N, Nicholas MG, Drevet B. Wettability at high temperatures. Pergamon, Oxford: Pergamon Materials Series; 1999.

26. Christian JW. The theory of phase transformation in metals and alloys. Oxford: Pergamon Press; 1965. p. 992.

27. Hall EO. The deformation and aging of mild steel. III. Discussion of result. Proc Phys Soc B. 1951;64:747–53.

28. Petch NJ. The cleavage strength of polycrystals. J Iron Steel Inst. 1953;174:25–8.

29. Ocak Y, Akbulut S, Boyuk U, Erol M, Keslioglu K, Marasli N. Solid–liquid interfacial energy for solid succinonitrile in equilibrium with succinonitrile dichlorobenzene eutectic liquid. Thermochim Acta. 2006;445:86–91.

30. Hunt JD, Jackson KA. Binary eutectic solidification. Trans Met Soc AIME. 1966;236:843–52.